

# Phosphate-Responsive Biomimetic Nanofluidic Diodes Regulated by Polyamine–Phosphate Interactions: Insights into Their Functional Behavior from Theory and Experiment

Gonzalo Pérez-Mitta,\* Waldemar A. Marmisollé, Alberto G. Albesa, María Eugenia Toimil-Molares, Christina Trautmann, and Omar Azzaroni\*

There is currently high interest in developing nanofluidic devices whose iontronic output is defined by biological interactions. The fabrication of a phosphate responsive nanofluidic diode by using the biological relevant amine–phosphate interactions is shown. The fabrication procedure includes the modification of a track-etched asymmetric (conical) nanochannel with polyallylamine (PAH) by electrostatic self-assembly. PAH is the archetypical model of polyamine and it is further used to address the nanochannels with phosphate responsivity. In order to explore the influence that phosphate in solution has in the conductance of the modified nanochannels, current–voltage measurements using different concentrations of phosphates are performed. Furthermore, to have a complete physicochemical understanding of the system, experimental data is analyzed using a continuous model based on Poison–Nernst–Planck equations and compared with results obtained from stochastic Monte Carlo simulations.

## 1. Introduction

The virtues of working with nanofluidic elements are being increasingly recognized by the nanoscience community, thus leading to the emergence of a research area that is currently at the forefront of materials science and engineering.<sup>[1]</sup> For instance, the advent of track-etching techniques (“top-down approach”) has resulted in an increasing mastery in the construction of nanoscale fluidic structures as well as the manipulation


of nanopore and nanochannel architectures with various shapes and diameters down to a few nanometers.<sup>[2]</sup> These research activities gave rise to design concepts to construct fully “abiotic” nanochannels with dimensions comparable to those of biological molecules.<sup>[3]</sup> One particular feature of these nanofluidic elements is their ability to display transport properties that resemble biological ion channels, such as ion selectivity, current rectification, flux inhibition by protons and divalent cations, transport of ions against concentration gradients, and even ion current fluctuations. In the case of asymmetric nanochannels/nanopores, appealing rectification effects arise when the channel surface is charged and the dimensions are comparable to the Debye

length,<sup>[4]</sup> thus leading to the emergence of nanochannel-based devices resting on surface charge governed ionic transport.

During the last decade, scientific community has thoroughly explored different types of (bio)chemical strategies to control the supramolecular, biological, and chemical nature of the pore walls.<sup>[5,6]</sup> In this regard, studying and exploiting the biological interactions of phosphates in confined environments is of high scientific relevance because phosphates are involved in the energy metabolism and are an important part of signaling molecules, nucleic acids, and lipids. Maintaining the total concentration of phosphates constant at around  $1.1 \times 10^{-3}$  M throughout the body is highly important for a number of cellular functions and many diseases are related to an excess or a deficit of the phosphate concentration in the cellular media. Due to this necessity of a fine control over the concentration for various physiological processes, there are several biological channels in charge of the transport of phosphates in and out the intracellular and the cellular media. Clear example of these protein channels is the sodium-phosphate cotransporter family SLC34.<sup>[7]</sup> These types of proteins are located in the small intestine and renal proximal tubules and are vital for the phosphate homeostasis.

Both the understanding of these confined processes and the designing of an artificial phosphate responsive nanofluidic device that mimics the phosphate transport proteins are of high scientific and technological interest.<sup>[8]</sup>

G. Pérez-Mitta, Dr. W. A. Marmisollé, Dr. A. G. Albesa, Prof. O. Azzaroni  
Instituto de Investigaciones Físicoquímicas Teóricas y Aplicadas (INIFTA)  
Departamento de Química, Facultad de Ciencias Exactas  
Universidad Nacional de La Plata (UNLP)  
CONICET, Boulevard 113 y 64, 1900 La Plata, Argentina  
E-mail: gperezmitta@inifta.unlp.edu.ar; azzaroni@inifta.unlp.edu.ar  
Dr. M. E. Toimil-Molares, Prof. C. Trautmann  
GSI Helmholtzzentrum  
64291 Darmstadt, Germany  
Prof. C. Trautmann  
Technische Universität Darmstadt  
64287 Darmstadt, Germany

 The ORCID identification number(s) for the author(s) of this article can be found under <https://doi.org/10.1002/sml.201702131>.

DOI: 10.1002/sml.201702131

It has been demonstrated that the synergistic combination of nanotechnology and supramolecular chemistry is a suitable mean to obtain cost-effective biomimetic functional materials with ease of production.<sup>[9]</sup> Several technological applications have already been produced specially for biosensing and energy conversion.<sup>[10,11]</sup> However, it is envisioned that further improvements in the control of surface properties of nanofluidic systems will create new opportunities to further modify the transport behavior for specific purposes and will lead to the development of a large set of nanofluidic technological devices in the forthcoming years.<sup>[12]</sup> For this reason, there is a large interest in improving the limited understanding of the physical-chemistry of confined responsive materials such as polyelectrolytes or polymer brushes and how they affect the concentration of ions inside nanopores or nanochannels. Mainly due to the complexity of obtaining experimental information of these systems, it is important to make additional use of different theoretical and computational techniques to provide a complete understanding of these systems.

In order to design a biomimetic phosphate-responsive device, the biological interactions of phosphates can serve as a source of inspiration. In this regard, one of the most important noncovalent interactions concerning inorganic phosphates is that with polyamines.<sup>[13]</sup> For example, complexes of polyamine and phosphates called nuclear aggregates of polyamines, and can be found within many cells.<sup>[14]</sup> These complexes are known to modulate changes in DNA molecules more effectively than single polyamines.<sup>[15]</sup> Also, this specific interaction of phosphate anions with amino groups of some membrane components has recently been suggested to play a crucial role in the modulation of the alternative functions of cytochrome in preapoptotic conditions.<sup>[16]</sup> P-NMR studies have revealed that interactions with phosphates occur in the whole range of pH where a typical synthetic polyamine, polyallylamine (PAH), is protonated and phosphate is anionic ( $\approx 4-9$ ).<sup>[17]</sup> On the other hand, this specific interaction between polyamines and phosphates was reported to reverse the surface charge in layer-by-layer polyelectrolyte multilayers.<sup>[18]</sup> Furthermore, the specific adsorption of phosphate anions onto amino-terminated self-assembled-monolayers, partially reversing the surface charge and even enhancing the adsorption of positively charged proteins, was demonstrated.<sup>[19]</sup>

Learning about the physicochemical nature of the interaction between phosphates and polyamines and how it behaves within nanoconfined environments is the first step in understanding these fundamental biological interactions and in devising new types of synthetic biosensors for phosphate-bearing molecules. Several modeling attempts have been performed by using different theoretical approaches.<sup>[20]</sup> Our group has found that a combination between a continuous model based on the equations of Poisson–Nernst–Planck (PNP) and a stochastic model using Monte Carlo (MC) simulations can provide valuable information about the influence of functional polyelectrolytes on the transport of ionic species in nanofluidic devices.

Herein, we study theoretically and experimentally the fabrication of bioinspired phosphate-responsive nanofluidic diodes based on the modification of a polymeric nanochannel by electrostatic self-assembly of PAH. The archetypical polyamine model PAH was extensively used to produce supramolecular

structures that resemble biological systems.<sup>[21]</sup> We found that the phosphate–polyamine interactions dictate the responsiveness of this nanofluidic device. The behavior of the ionic current in solutions with different concentrations of phosphate anions showed a monotonic trend. To have a complete physicochemical understanding of the system, theoretical analysis was performed using a continuous transport model based on the Poisson–Nernst–Planck equations and an ion-binding study based on Monte Carlo simulations. This theoretical analysis led to a good understanding of the experimental results.

## 2. Results and Discussion

In order to study the conductance of the track-etched nanochannels,  $I-V$  curves were recorded. The conductance of the bullet-shaped nanochannels did not show ohmic behavior but presented a cation selective rectified transport. This effect is ascribed to the asymmetry in charge density along the nanochannels.<sup>[22–24]</sup>

As previously reported, the rectification behavior of asymmetric nanochannels is highly dependent on the surface charge and the nanometric size of the nanochannel. This is due to the electrostatic selectivity toward a certain type of ion that stems from the difference between the electric potential profiles that result from the superposition of the electric potential distribution of the channel and applied transmembrane potentials.<sup>[25]</sup> If the charge is switched from positive to negative, the system changes from anion to cation-selective,<sup>[26]</sup> and consequently, the rectification of the ionic current becomes reverted as well. This modulation of the current rectification is of high importance for technological applications, especially for biosensing.<sup>[27,28]</sup>

Once the  $I-V$  curves for the etched channels were measured, the nanochannels were functionalized with PAH by dip coating. After the modification the foil was rinsed several times and left to dry in ambient conditions before performing the measurements. Due to the positive amino functional groups present in the PAH units the direction of the rectification was reverted after the modification (Figure S1, Supporting Information). The as-modified single-nanochannel membranes were then reinserted in the conductivity cell and  $I-V$  curves were measured in the presence of different concentrations of phosphate anions (Figure 1a). The experiments were conducted at pH 7 where significant changes of the rectification behavior due to phosphates can be observed.  $I-V$  curves reveal the binding of phosphates on the polyamine-modified nanochannel by changes in the overall  $I-V$  behavior and in the rectification efficiency. Total phosphate concentrations (Pi) up to  $50 \times 10^{-3}$  M were used, finding a strong reversion in the rectification.

At low concentrations of phosphates, the nanochannel behaves in an anion-selective way and the rectification occurs toward negative potentials, meaning that the low conductance state is for positive potentials, while the high conductance state is at negative potentials. By increasing the concentration of phosphates, the rectification starts to fade leading to an ohmic (linear) behavior that is reached at a concentration of  $2.5 \times 10^{-3}$  M. For higher concentrations an inversion of the rectification is observed and the behavior becomes cation-selective,

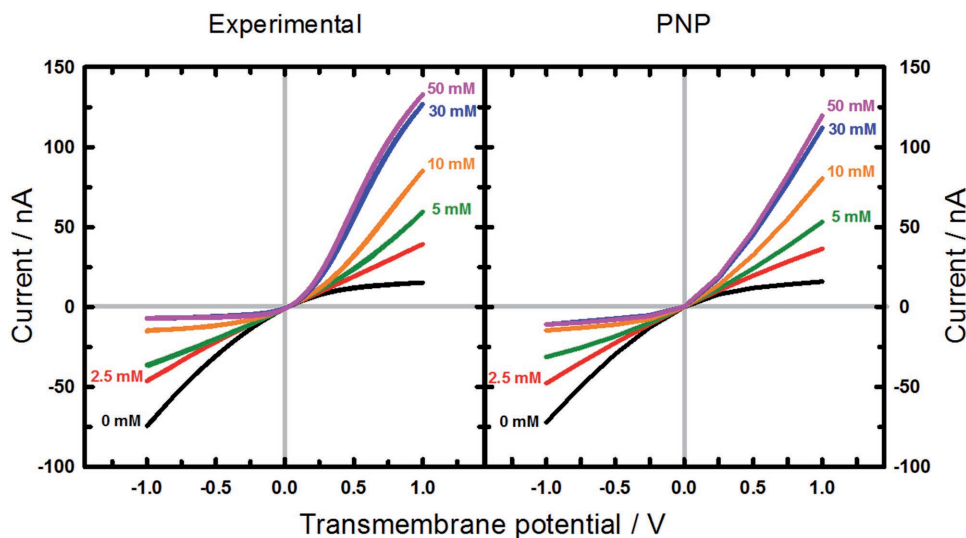


**Figure 1.** a)  $I$ - $V$  curves of PAH-modified nanochannel under different concentrations of phosphate in 0.1 M KCl solution at pH 7.00. A strong reversion is observed at high concentrations of phosphate. b) PNP simulations of the  $I$ - $V$  curves with different phosphate (Pi) concentrations.

where the lower conductance state is at negative and the higher at positive potentials.

As the phosphate concentration also contributes to the conductivity of the solution it was important to differentiate the effects in the  $I$ - $V$  curves stemming from changes in the surface charge density from the effects due to the increase of the solution conductivity. To achieve this goal, we analyzed the experiments using a continuous model based on the Poisson-Nernst-Planck equations (Figure 1b). Information about the modeling can be found in the Supporting Information.

The PNP model allows comparing surface charge density values for each different experimental  $I$ - $V$  curve by using a fixed set of geometric values (base, tip diameter, form factor). The results of the modeling performed for each concentration showed that the surface charge density decreases in magnitude until a concentration of  $2.5 \times 10^{-3}$  M (zero charge point,  $\approx 0.1$  e nm $^{-2}$ ) and then it increases again but with an opposite sign (Figure 2, red curve). The PNP theory shows that the slight difference between the curves at 30 and  $50 \times 10^{-3}$  M is related

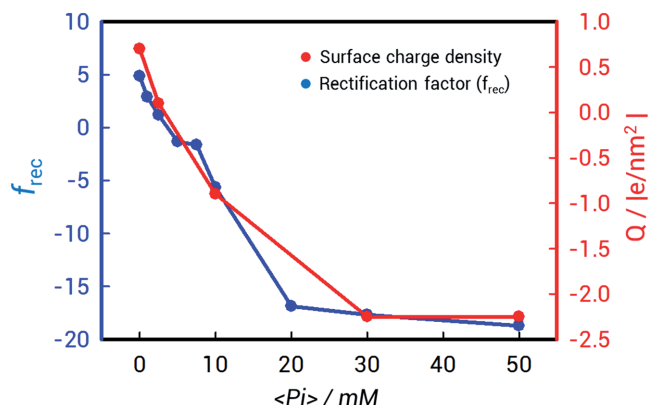


**Figure 2.** Rectification efficiency and surface charge of a PAH modified nanochannel as obtained from the PNP theory. Results show the correspondence between the rectification factor and the surface charge density.

to the change in the solution's conductivity and not to a different charge state. Figure 2 shows the close relation that exists between the behavior of the rectification factor and the surface charge density, as a function of the Pi concentration. Therefore, changes in the  $f_{rec}$  for a particular nanochannel can be ascribed to changes in the surface charge for discussion purposes.

In order to further verify the binding of the phosphates to the PAH and the reversion of surface charge, independent zeta-potential measurements with PAH-modified silicon dioxide nanoparticles were performed. Results showed a similar trend of the zeta potential with the concentration of phosphates in solution, confirming the reversion of the surface charge ( $f_{rec}$ ) with increasing phosphate concentrations (Figure S2, Supporting Information).

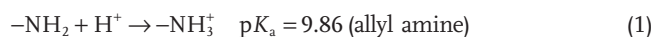
### 3. Monte Carlo Simulations

The effect of confinement on the physicochemical interactions between polyamines and phosphates was investigated by MC simulations using nanochannels of different diameters. We simulate open nanochannels with diameters of 10, 20, and 30 nm and a length of 20 nm. A polymer density of 0.1 chains nm $^{-2}$  was held constant for the simulations. To attain this, channels were simulated using 72, 144, and 216 polymer chains, respectively. Each chain was formed for 10 monomeric units with a radius of 0.3 nm. The excluded volume was taken into account by considering a hard sphere potential between the monomers and the ions and the conformational search was performed by allowing the monomers in the chain to rotate around a random angle between  $\pi$  and  $2\pi$ .

In this model we consider only electrostatic interactions. Therefore, these results can be applied also for other divalent species. However, it is important to mention that it has been previously shown that amine interactions are stronger with phosphates than with other divalent species.<sup>[29,30]</sup> Due to the fact that simulations do not acknowledge the chemical nature

of each ion but only its charge, we will refer to the ionic species generically as cations (potassium ions), monovalent anions (which include chloride and dihydrogen phosphate ions), and divalent anions (hydrogen phosphate ions) when speaking about the MC simulations.

The monomer units in the polymer have the following acid–base equilibrium:



The acidic behavior was investigated within a grand canonical ensemble. A monomer was picked randomly and an attempt was made to switch its charge state. The change in (free) energy ( $\Delta E$ ) governing the success of the attempt was composed by the change in the coulombic interactions between monomers, cations, and anions ( $\Delta E_{\text{total}}$ ) and the free energy change corresponding to the acid–base reaction of an isolated monomer:<sup>[31,32]</sup>

$$\Delta E = \Delta E_{\text{total}} \pm k_B T \ln 10(\text{pH} - \text{p}K_a) \quad (2)$$

where pH is the pH of the system and  $\text{p}K_a$  the intrinsic  $\text{p}K_a$  of a monomer. The plus sign indicates that the monomer is to be protonated, and the minus sign that it is to be deprotonated.

**Figure 3** shows the concentration of each ionic species inside the channel with respect to the concentration of the divalent salt in bulk calculated with MC simulations for the channel before (bare) and after the functionalization with PAH and also for three different channel diameters: 10, 20, and 30 nm. Concentrations inside the pores were calculated dividing the total sum of each specie units by the volume of the channel.

Since the bare channels are negatively charged, cations are electrostatically attracted while anions are repelled, thus producing a concentration polarization, i.e., an increase in the concentration of cations inside the channels as well as a decrease in the anion concentration. Even though this general tendency is observed for the three different sizes, the difference between cation and anion concentrations becomes smaller with increasing channel diameter, which is consistent with the known fact that there is a lower overlapping of electrical double layer stemming from the surface due to the larger size.<sup>[33]</sup>

Figure 3 shows that the concentration of cations and divalent anions inside bare channels increases with higher bulk concentration, while the monovalent anion concentration remains almost constant. These results are consistent with our previous results where it was experimentally shown that for negatively charged nanochannels at low concentrations, the contribution to the ionic current of double charged anions is similar to the contribution of monovalent anions; meaning that there are similar concentrations of both species within the channels. However, for higher concentration the contribution of double charged anions is higher than that of monovalent anions.<sup>[34]</sup> For example, the contribution of divalent anions is almost the same as the contribution of monovalent anions at a concentration of  $50 \times 10^{-3} \text{ M}$  but twofold at  $100 \times 10^{-3} \text{ M}$ .

After the channels were functionalized with PAH, the concentration profiles change radically. The change in the profiles accounts for changes in the surface charge, from negative to positive, but also for the interaction between the PAH and the

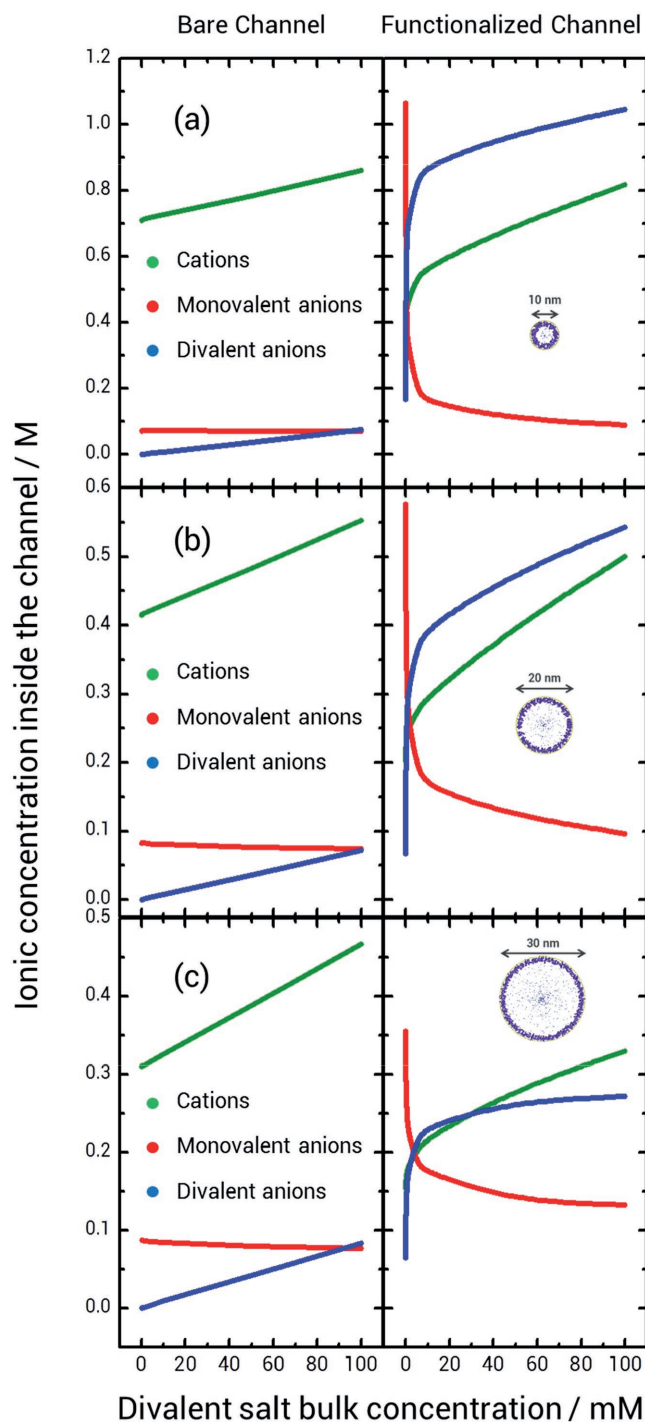


**Figure 3.** Ionic concentrations of each ionic specie inside a channel of diameter of a) 10 nm, b) 20 nm, and c) 30 nm as a function of the concentration of divalent salt in bulk. Images of the modified nanochannels as obtained from the MC simulations are shown in right panels.

divalent anions. The relation between these two factors determines the relation between the concentration profiles as a function of divalent salt bulk concentrations (DBC) and nanochannel sizes.

There are two main observations that can be made from the concentration profiles at the three channels diameters.

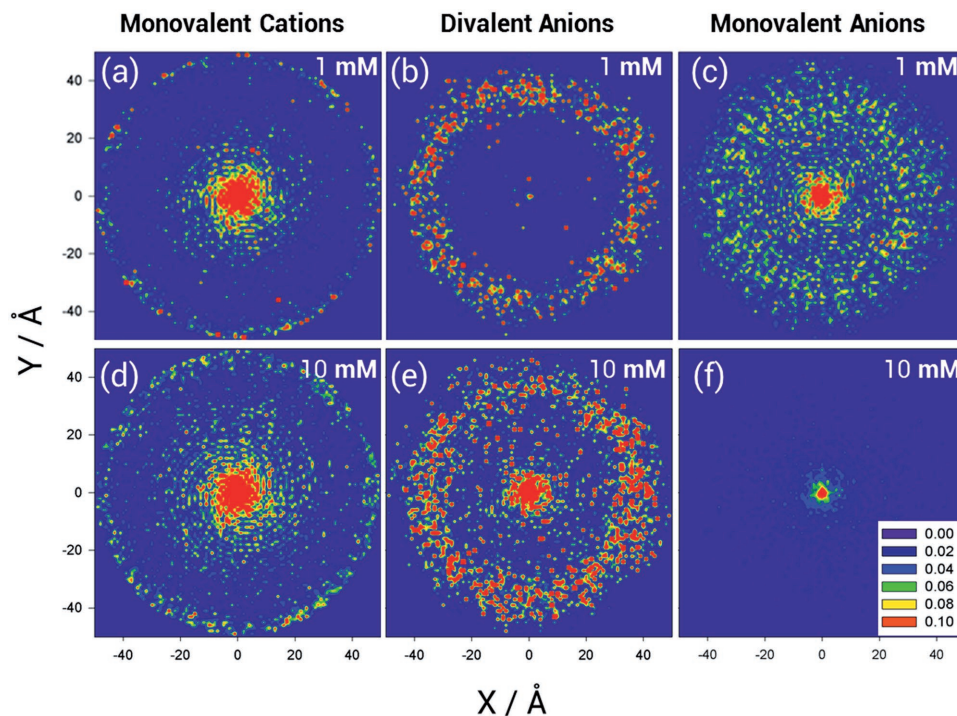


**Figure 4.** 2D ionic distribution inside a 10 nm diameter channel at a divalent salt bulk concentration of a–c)  $1 \times 10^{-3}$  M and d–f)  $10 \times 10^{-3}$  M.

First, the concentration of divalent anions and cations increases steeply with the DBC, while the monovalent anion decreases. This decrease of monovalent anions inside the channels (due to electrostatic repulsions) explains the change in the direction of the rectification observed in the experimental  $I$ – $V$  curves at a Pi concentration of  $2.5 \times 10^{-3}$  M or zero charge point (ZCP). At the ZCP, the amount of divalent anions is enough to neutralize the net positive charge stemming from the PAH. This point is observed in the concentration profiles where the curves for monovalent cations and anions cross (no ionic selectivity). Despite the electrostatic neutralization, higher amounts of divalent anions (Pi for  $I$ – $V$  curves) can still bound to the PAH shifting the surface charge to more negative values, and consequently decreasing the concentration of anions inside the channels. Further corroboration of this effect can be obtained from the radial distribution of each different ion within the pore (Figure 4). Figure 4 shows that changing the DBC from 1 to  $10 \times 10^{-3}$  M produces a large increment in divalent anions on the surface of the nanochannel, while the quantity of monovalent anions is largely reduced. For the sake of comparison, the radial distribution of ionic species for bare channels can be found in Figure S3 of the Supporting Information.

The second general observation is that the concentration profiles of each species follow an asymptotic behavior with the DBC, which is also consistent with experimental values. Experimentally measured rectification factors (or equivalently, surface charge density) saturate at a concentration of  $\approx 20 \times 10^{-3}$  M (Figure 2), which means that the amount of phosphates that can be bound to the surface is maximum at this concentration and so it is the negative surface charge. In this regard, MC simulations show saturation on the divalent anion concentration

inside the channels at a bulk concentration of  $\approx 30 \times 10^{-3}$  M (Figure 3).

Another interesting feature is that, even though the general trend was that the concentration of divalent anions was higher than that of monovalent cations, this trend is not sustained for bulk concentration higher than  $\approx 50 \times 10^{-3}$  M for 30 nm diameter channels, where the concentration profiles for the divalent anion and cation showed a cross-over. For bulk concentrations higher than this crossing point, the relation between these profiles is reverted. Such feature was not observed for the 10 and 20 nm channels, being the current of cations higher than for divalent anions.

Since double charged anions are located over the surface of the channel due to strong interactions (Figure 4), they contribute to maintain a net negative charge over the surfaces making the channel cation selective. Therefore, it is expected for the cation concentration to increase with the bulk concentration due to the electrostatic attraction. However, due to the fact that the layer of divalent anions is about 2 nm thick and cations are mainly concentrated to the center of the pore (Figure 4), an entropic constraint for the increment of cation concentration within smaller pores is generated.

In order to fully understand the experimental results it is important to consider the chemical changes of the polyamine layer. In this regard, due to the fact that the MC simulations consider the acid–base equilibrium of the monomers, the protonation degree of the polyamine as a function of the concentrations of the divalent salt could be calculated (Figure 5).

The protonation degree of PAH as a function of the divalent anion bulk concentrations was calculated for three different channel diameters, 10, 20, and 30 nm. Again, a distinctive behavior was found for the 30 nm channel for which the

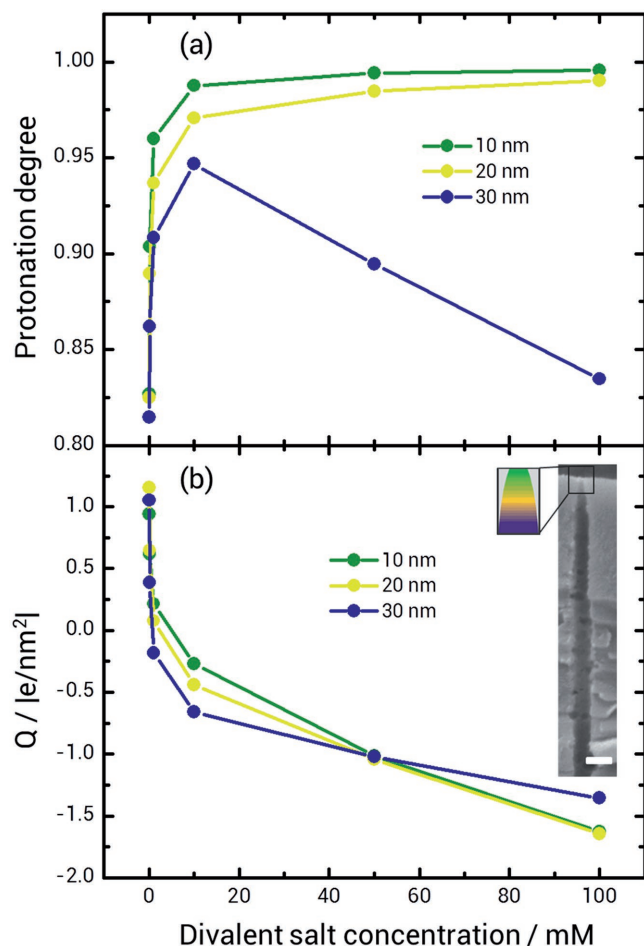


**Figure 5.** a) Protonation degree for a PAH inside three different channels of a diameter of 10 nm (green), 20 nm (yellow), and 30 nm (blue) as function of the divalent salt concentration in bulk. b) Surface charge density ( $q$ ) as a function of the divalent salt concentration for three different channels of diameters of 10 nm (green), 20 nm (yellow), and 30 nm (blue). The inset figure on the right shows a scheme for an asymmetric channel with a color code related to the curves to represent the change in the size dependent properties and a cross-section Scanning Electron Microscopy (SEM) image of the bullet-shaped channels. Scale bar, 1  $\mu$ m.

protonation degree steeply increases up to a concentration of  $10 \times 10^{-3}$  M and then decreases in a linear fashion. At a bulk concentration below or equal to  $10 \times 10^{-3}$  M, the polymer shows an increment of the protonation degree on the concentration which responds to a preference to be in a positive charged state in order to minimize electrostatic repulsions by interacting with the anions present in solution. However, at concentrations higher than  $10 \times 10^{-3}$  M the protonation degree starts to decrease, which can be understood as the prevalence of entropy from both the dissolved anions and deprotonated polymer over the electrostatic interactions. Conversely, for the case of 10 and 20 nm diameter channels, the protonation degree increases monotonically with the bulk concentration. For these two diameters there is greater confinement of the species, therefore, for the energy balance, electrostatic interactions become more relevant than the entropic contribution and as a consequence the polymer remains in a highly protonated state even at high bulk concentrations.

The MC simulations using different diameters can be used to envision changes along an asymmetrically shaped nanochannel of the ion distribution and the PAH protonation degree by thinking each simulation as a cross-section of a different diameter from a nanochannel, as shown in the scheme in Figure 5b, the closest to the tip the smaller the diameter.

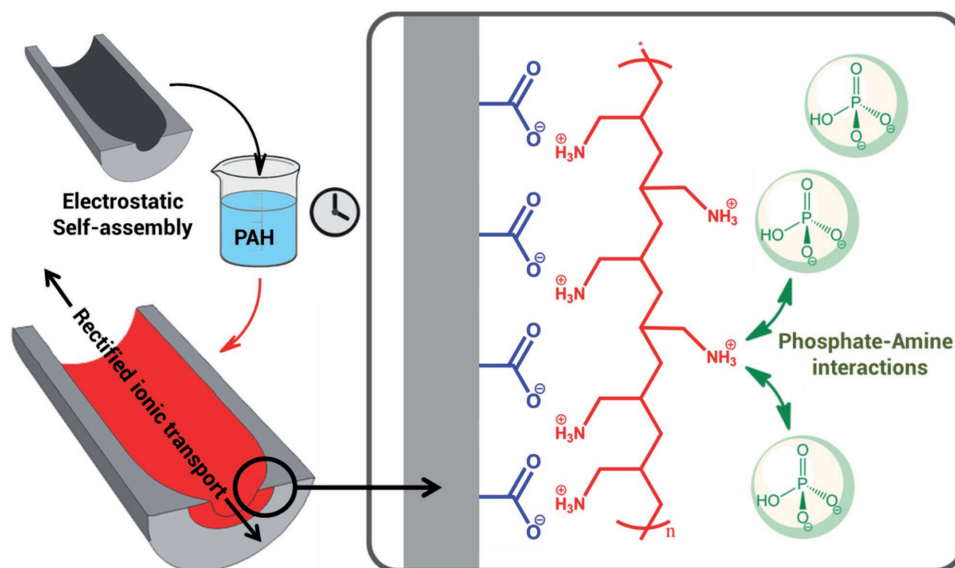
Using this model, we can argue that there is a nonhomogeneous distribution of charge along the channels due to a different protonation degree of the PAH at different diameters with a high density of positive charges localized near the tip of the channels (Figure 5a, green curve), especially at high divalent salt concentration. This observation is interesting because it shows that increasing confinement of the system can result in the amplification of the response of a molecule (PAH) to a stimulus (concentrations of divalent anions) which could be of paramount importance for designing biosensing or nanofluidic devices. It is also interesting because it seems to contradict the hypothesis of homogeneous distribution of charge used for the PNP model. In order to compare the results from both theoretical approaches and also to address the influence of size in the charge distribution, the surface charge density from the net charge inside the channel was obtained from the MC data (Figure 5b).

The net charge inside the channel was calculated as the number of positive charges from the polymer minus twice the number of divalent anions minus the charge in the wall. By doing this, the assumption that all the divalent anions are bound to the polymer was made. The charge density in the wall prior to the modification with PAH, due to the carboxyl groups, was  $-1.0 |e/nm^2|$ . Figure 5b presents the calculated surface charge density for PAH modified channels of different diameters. Results show that there is not a significant difference in the charge densities between channels of different diameters. By performing these calculations, it can be seen that the charge densities calculated for different bulk concentrations using MC calculations and the values found experimentally and with the PNP theory show a good qualitative agreement (Figures 2 and 5b) taking into account the difference between the simulated systems.

#### 4. Conclusions

We presented a phosphate-responsive nanofluidic diode based on the functionalization of solid-state nanochannels with PAH. PAH is a polyamine, a family of polymers that can be used as models for highly relevant biochemical processes especially due to their capacity to strongly interact with phosphates. Experimental results showed that the ionic transport characteristics of the channels can be fine-tuned by using different concentrations of inorganic phosphates to modulate the surface charge of the channels. Additionally, zeta-potential measurements were made in PAH-modified  $SiO_2$  nanoparticles in order to corroborate the trend of the surface charge toward increasing Pi concentrations.

To have a deep insight over the physical chemistry of the system, theoretical simulations using continuous Poisson-Nernst-Planck and stochastic Monte Carlo models were performed. The results show that there is a complex interaction



**Scheme 1.** Surface functionalization procedure with PAH and detail of the interactions present in the system.

between the polyamine and phosphate counterions to determine the ionic concentration profiles inside the channels. Simulations showed that the divalent phosphates are mostly concentrated toward the walls of the channels, ultimately changing the charge of the walls and therefore producing an increase in the selectivity of the channels to cations with increasing phosphate concentrations. Monte Carlo simulations performed using different channel diameters showed that protonation degree of the PAH increases due to the confinement and the phosphate concentration up to a certain diameter and also that the concentration of phosphates is adjusted in order to achieve a similar charge density for different diameters.

## 5. Experimental Section

**Chemical Etching:** Polyethylene terephthalate (PET) foils irradiated with one single heavy ion were chemically etched creating a “bullet-like” shaped open channel. Details of the surfactant-assisted etching process performed in a two-chamber electrolytic cell are explained elsewhere.<sup>[35–37]</sup> Before the etching process, the ion-track containing foils were exposed on one side to UV light for 6 h only on the side exposed to the etchant without surfactant. Chamber (1) of the etching cell was filled with 6 M NaOH as etching solution, while 0.05% (in volume) of the anionic surfactant Dowfax 2a1 was added to the etchant in chamber (2). The UV-treated foil surface was mounted toward cell chamber (1). The etching time was 6.5 min at a temperature of 60 °C.

**Nanochannel Functionalization:** PAH (≈58 kDa) was purchased from Sigma-Aldrich and used as received.

The track-etched foils were immersed in a  $10 \times 10^{-3}$  M solution of PAH (in monomeric units) at pH 6.00 for 1 h (**Scheme 1**). Subsequently, the foils were rinsed several times with deionized water and left to dry in air before performing the measurements.

**Conductivity Measurements:** I–V curves were measured using a potentiostat Reference 600 from Gamry. A four electrode set-up was used. The voltage was swept between –1 and 1 V at  $100 \text{ mV s}^{-1}$ . All experiments were performed using 0.1 M solutions of KCl. The pH value was kept constant by adding  $5 \times 10^{-3}$  M HEPES solution to adjust the pH to 7.  $\text{K}_2\text{HPO}_4$  was added up to concentrations of  $50 \times 10^{-3}$  M taking care of

regulating the pH to 7. HEPES, KCl, and  $\text{K}_2\text{HPO}_4$  were purchased from Sigma-Aldrich, Anedra, and Carlo Erba, respectively, and used as received.

**Rectification Rate:** The rectification efficiency was calculated as the ratio between the absolute values of the currents recorded at 1 and –1 V. The current in the denominator is always the one with lower conductance. If the current in the nominator is positive, the result is multiplied by –1 so that a positive rectification rate is associated with a positive surface charge and a negative rectification with a negative surface charge.

## Supporting Information

Supporting Information is available from the Wiley Online Library or from the author.

## Acknowledgements

The authors acknowledge financial support from the Deutsche Forschungsgemeinschaft (DFG-FOR 1583), CONICET (PIP0370), and ANPCyT (PICT-2013-0905, PICT-2016-1680). G.P.-M. acknowledges CONICET for a doctoral fellowship. W.A.M., A.G.A., and O.A. are staff members of CONICET. M.E.T.-M. and C.T. acknowledge support by the LOEWE project iNAPO funded by the Hessen State Ministry of Higher Education, Research and Arts.

## Conflict of Interest

The authors declare no conflict of interest.

## Keywords

biosensing, iontronics, nanofluidics, solid-state nanopores, supramolecular chemistry

Received: June 22, 2017

Revised: August 9, 2017

Published online:

- [1] a) B. E. B. Kalman, I. Vlasiouk, Z. S. Siwy, *Adv. Mater.* **2008**, *20*, 293; b) Z. Siwy, Y. Gu, H. A. Spohr, D. Baur, A. Wolf-Reber, R. Spohr, P. Apel, Y. E. Korchev, *Europhys. Lett.* **2002**, *60*, 349; c) Y. He, D. Gillespie, I. Vlasiouk, R. S. Eisenberg, Z. S. Siwy, *J. Am. Chem. Soc.* **2009**, *131*, 5194; d) P. Actis, A. C. Mak, N. Pourmand, *Bioanal. Rev.* **2010**, *1*, 177; e) B. Vilozny, P. Actis, R. A. Seger, N. Pourmand, *ACS Nano* **2011**, *5*, 3191; f) P. Actis, A. McDonald, D. Beeler, B. Vilozny, G. Millhauser, N. Pourmand, *RSC Adv.* **2012**, *2*, 11638.
- [2] a) P. Apel, *Radiat. Meas.* **2001**, *34*, 559; b) P. Y. Apel, I. V. Blonskaya, O. L. Orelovitch, P. Ramirez, B. A. Sartowska, *Nanotechnology* **2001**, *22*, 175302; c) P. Y. Apel, I. V. Blonskaya, O. L. Orelovitch, B. A. Sartowska, R. Spohr, *Nanotechnology* **2012**, *23*, 225503; d) L. Samoilova, P. Y. Apel, *Radiat. Meas.* **1995**, *25*, 717; e) Z. Siwy, P. Apel, D. Baur, D. D. Dobrev, Y. E. Korchev, R. Neumann, R. Spohr, C. Trautmann, *Surf. Sci.* **2003**, *535*, 1061; f) X. Hou, H. Dong, D. Zhu, L. Jiang, *Small* **2010**, *6*, 361; g) Y. Zhang, X. Y. Kong, L. Gao, Y. Tian, L. Wen, L. Jiang, *Materials (Basel)*. **2015**, *8*, 6277.
- [3] a) X. Hou, L. Jiang, *ACS Nano* **2009**, *3*, 3339; b) X. Hou, W. Guo, L. Jiang, *Chem. Soc. Rev.* **2011**, *40*, 2385.
- [4] a) J. Cervera, P. Ramirez, S. Mafe, P. Stroeve, *Electrochim. Acta* **2011**, *56*, 4504; b) J. Cervera, B. Schiedt, R. Neumann, S. Mafé, *J. Chem. Phys.* **2006**, *124*, 104706.
- [5] a) Z. Siwy, E. Heins, C. C. Harrell, P. Kohli, C. R. Martin, *J. Am. Chem. Soc.* **2004**, *126*, 10850; b) G. Pérez-Mitta, W. Marmisollé, C. Trautmann, M. E. Toimil-Molares, O. Azzaroni, *Adv. Mater.* **2017**, *29*, 1700972; c) B. Yameen, M. Ali, R. Neumann, W. Ensinger, W. Knoll, O. Azzaroni, *Chem. Commun.* **2010**, *46*, 1908; d) G. Pérez-Mitta, J. S. Tuninetti, W. Knoll, C. Trautmann, M. E. Toimil-Molares, O. Azzaroni, *J. Am. Chem. Soc.* **2015**, *137*, 6011; e) B. Yameen, M. Ali, R. Neumann, W. Ensinger, W. Knoll, O. Azzaroni, *J. Am. Chem. Soc.* **2009**, *131*, 2070; f) M. Ali, B. Yameen, J. Cervera, P. Ramírez, R. Neumann, W. Ensinger, W. Knoll, O. Azzaroni, *J. Am. Chem. Soc.*, **2010**, *132*, 8338.
- [6] a) Z. Meng, H. Bao, J. Wang, C. Jiang, M. Zhang, J. Zhai, L. Jiang, *Adv. Mater.* **2014**, *26*, 2329; b) L. Wen, Q. Liu, J. Ma, Y. Tian, C. Li, Z. Bo, L. Jiang, *Adv. Mater.* **2012**, *24*, 6193; c) N. Liu, Y. Jiang, Y. Zhou, F. Xia, W. Guo, L. Jiang, *Angew. Chem., Int. Ed.* **2013**, *52*, 2007; d) M. Zhang, X. Hou, J. Wang, Y. Tian, X. Fan, J. Zhai, L. Jiang, *Adv. Mater.* **2012**, *24*, 2424.
- [7] H. Murer, I. Forster, J. Biber, *Eur. J. Physiol.* **2004**, *447*, 763.
- [8] H. Zhang, Y. Tian, L. Jiang, *Nanotoday* **2016**, *11*, 61.
- [9] K. Xiao, L. Wen, L. Jiang, *Small* **2016**, *12*, 2810.
- [10] Y. Wang, K. Kececi, M. V. Mirkin, V. Mani, N. Sardesai, J. F. Rusling, *Chem. Sci.* **2013**, *4*, 655.
- [11] H. Dong, R. Nie, X. Hou, P. Wang, J. Yue, L. Jiang, *Chem. Commun.* **2011**, *47*, 3102.
- [12] A. van den Berg, H. G. Craighead, P. Yang, *Chem. Soc. Rev.* **2010**, *39*, 899.
- [13] M. Sumper, *Angew. Chem., Int. Ed.* **2004**, *43*, 2251.
- [14] L. D'Agostino, A. di Luccia, *Eur. J. Biochem.* **2002**, *269*, 4317.
- [15] L. D'Agostino, M. di Pietro, A. Di Luccia, *FEBS J.* **2005**, *272*, 3777.
- [16] D. A. Capdevila, W. A. Marmisollé, F. Tomasina, V. Demicheli, M. Portela, R. Radi, D. H. Murgida, *Chem. Sci.* **2015**, *6*, 705.
- [17] K. Lutz, C. Gröger, M. Sumper, E. Brunner, *Phys. Chem. Chem. Phys.* **2005**, *7*, 2812.
- [18] J. Irigoyen, S. E. Moya, J. J. Iturri, I. Larena, O. Azzaroni, E. Donath, *Langmuir* **2009**, *25*, 3374.
- [19] W. A. Marmisollé, D. A. Capdevila, E. De Llave, F. J. Williams, D. H. Murgida, *Langmuir* **2013**, *29*, 5351.
- [20] M. Tagliacuzzi, I. Szeleifer, *Soft Matter* **2012**, *8*, 7292.
- [21] W. A. Marmisollé, J. Irigoyen, D. Gregurec, S. Moya, O. Azzaroni, *Adv. Funct. Mater.* **2015**, *26*, 4144.
- [22] Z. Siwy, A. Fulinski, *Am. J. Phys.* **2004**, *72*, 567.
- [23] R. Karnik, C. Duan, K. Castelino, H. Dajugui, A. Majumdar, *Nano Lett.* **2007**, *7*, 547.
- [24] H. S. White, A. Bund, *Langmuir* **2008**, *24*, 2212.
- [25] Z. Siwy, E. Heins, C. C. Harrell, P. Kohli, C. R. Martin, *J. Am. Chem. Soc.* **2004**, *126*, 10850.
- [26] B. Yameen, M. Ali, R. Neumann, W. Ensinger, W. Knoll, O. Azzaroni, *J. Am. Chem. Soc.* **2009**, *131*, 2070.
- [27] S. Howorka, Z. Siwy, *Chem. Soc. Rev.* **2009**, *38*, 2360.
- [28] B. Vilozny, A. L. Wollenberg, P. Actis, D. Hwang, B. Singaram, N. Pourmand, *Nanoscale* **2013**, *5*, 9214.
- [29] D. A. Capdevila, W. A. Marmisollé, F. J. Williams, D. H. Murgida, *Phys. Chem. Chem. Phys.* **2013**, *15*, 5386.
- [30] W. J. Dressick, K. J. Wahl, N. D. Bassim, R. M. Stroud, D. Y. Petrovykh, *Langmuir* **2012**, *28*, 15831.
- [31] F. Carnal, S. Stoll, *J. Phys. Chem. B* **2011**, *115*, 12007.
- [32] S. A. Barr, A. Z. Panagiotopoulos, *J. Chem. Phys.* **2012**, *137*, 144704.
- [33] R. Schoch, J. Han, Renaud, *Rev. Mod. Phys.* **2008**, *80*, 839.
- [34] G. Pérez-Mitta, A. G. Albesa, M. E. Toimil-Molares, C. Trautmann, O. Azzaroni, *ChemPhysChem* **2016**, *17*, 2718.
- [35] G. Pérez-Mitta, J. S. Tuninetti, W. Knoll, C. Trautmann, M. E. Toimil-Molares, O. Azzaroni, *J. Am. Chem. Soc.* **2015**, *137*, 6011.
- [36] G. Pérez-Mitta, A. G. Albesa, W. Knoll, C. Trautmann, M. E. Toimil-Molares, O. Azzaroni, *Nanoscale* **2015**, *7*, 15594.
- [37] P. Y. Apel, I. V. Blonskaya, S. N. Dmitriev, O. L. Orelovitch, A. Presz, B. A. Sartowska, *Nanotechnology* **2007**, *18*, 305302.